Apparatus to measure the vapor pressure of slowly decomposing compounds from 1 Pa to 10^5 Pa

Robert F. Berg

robert.berg@nist.gov

Sensor Science Division
National Institute of Standards and Technology
Gaithersburg, Maryland, 20899-8411

22 October 2015

Abstract

This article describes an apparatus and method for measuring vapor pressures in the range from 1 Pa to 10^5 Pa. Its three distinctive elements are: (1) the static pressure measurements were made with only a small temperature difference between the vapor and the condensed phase, (2) the sample was degassed *in situ*, and (3) the temperature range extended up to 200 °C. The apparatus was designed to measure metal-organic precursors, which often are toxic, pyrophoric, or unstable. Vapor pressures are presented for naphthalene, ferrocene, diethyl phthalate, and TEMAH (tetrakisethylmethylaminohafnium). Also presented are data for the temperature-dependent decomposition rate of TEMAH.

1. Introduction

Making a modern microprocessor requires half of the elements in the periodic table, many of which are metals that are used in features such as conducting lines (Cu), dielectric layers (HfO_2), and diffusion barriers (TaN). The metal often arrives at the silicon wafer as the vapor of a metal-organic precursor, and the chemists who design the precursor must compromise between a large vapor pressure and other desirable properties such as thermal stability [1]. Knowing the precursor's vapor pressure is useful because it determines the behavior of the vapor delivery device.

The present apparatus was built for metal-organic precursors, which are typically used at temperatures from 20 °C to 200 °C and can have vapor pressures in the range from 1 Pa to 10^5 Pa. They are often toxic, pyrophoric, or unstable, so the apparatus included safety features, and the measurements and analysis allowed for the possibility of slow decomposition. The apparatus and method had three distinctive elements: (1) the static pressure measurements were made with only a 1 K temperature difference between the vapor and the condensed phase, (2) the sample was degassed *in situ*, and (3) the temperature range extended up to 200 °C.

Reviews of techniques to measure the vapor pressure of pure liquids and solids include articles or chapters by Ambrose [2,3], Verevkin [4], Růžička et al. [5], Raal and Ramjugernath [6], and Raal and Mühlbauer [7]. Verevkin mentions five methods to measure vapor pressure: ebulliometric, effusion, static, transpiration, and calorimetric. The ebulliometric (boiling) method is accurate because it can precisely compare the unknown vapor pressure of a liquid to the known vapor pressure of a reference liquid; however, it has difficulties below 1 kPa [5], and the samples must be liquid and relatively large (~10 cm^3). The effusion method, which measures the force or the mass loss due to the ejection of vapor from a sample holder, uses only a small sample; however, it requires a mean free path of at least a few mm, which makes it unsuitable above 10 Pa. Of the remaining methods, the static method used here is the most accurate [5], and it can be applied at any pressure for which one has a suitable sensor, from less than 1 Pa to more than 10 MPa. Examples of static method apparatuses can be found in References [8-15].

The static method is simply a measurement of the pressure of vapor in equilibrium with a condensed sample. It requires steady conditions, with the sample located at the coldest part of the manifold; otherwise, evaporation and condensation slowly move the sample and cause drift of the measured pressure. The usual practice is to hold the pressure gauge at a high, fixed temperature while varying the sample temperature (Figure 1a). A less common, alternate practice is to maintain a fixed difference between the temperatures of the pressure gauge and the sample (Figure 1b). The alternate practice was implemented here by putting both the sample and the pressure gauge into a temperature-controlled oven and using a thermoelectric device [16] to control the sample temperature T_{sample}. The oven varied the temperature T_{air} of the air surrounding the pressure gauge, and the device cooled the sample by the fixed difference $T_{air} - T_{sample}$. Keeping the temperature difference small reduced problems caused by thermal transpiration at low pressures, and it decreased the decomposition rate of the vapor for unstable samples.

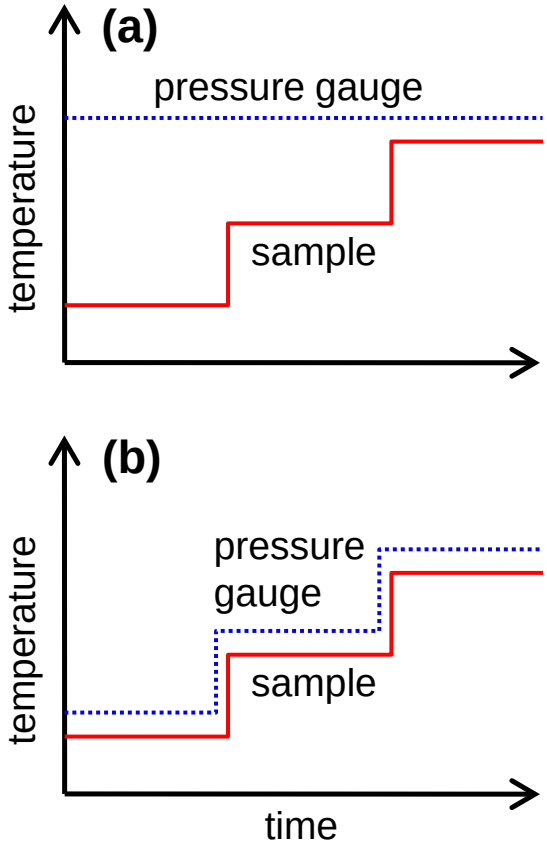

Figure 1. Two practices for measuring vapor pressure as a function of temperature. (a) Usual: The temperature of the pressure gauge is held at a higher, fixed temperature, while the sample temperature varies. (b) Alternate: The difference between the two temperatures is fixed. The temperature of the pressure gauge was stepped before that of the sample.

The sample volume was small, about 1 cm^3, which reduced the risk of an accident and the costs of handling a toxic or pyrophoric sample. A small sample also can be degassed more quickly. Degassing the sample while it is in the apparatus eliminated the need for a separate distillation apparatus, and it allowed the sample to be measured immediately after it was degassed. *In situ* degassing is especially useful for a decomposing sample because volatile decomposition products can be removed between sets of vapor pressure measurements.

The remainder of this article describes the apparatus, its operation, and the results obtained for four compounds. A companion article [17] discusses the causes of time dependence in the pressure measurements.

2. Apparatus

2.1 Hot manifold

As shown in Figure 2 and Figure 3, the apparatus had two gas manifolds, a hot manifold contained in a convection oven and a room temperature manifold. The hot manifold comprised the sample tube, two capacitance diaphragm pressure gauges (CDG), and a cold trap, all of which were connected by pneumatic valves and metal gasket fittings (1/4 inch (6 mm) silver-plated nickel VCR [18]). The sample tube was surrounded by an aluminum block fitted with a thermistor, a platinum resistance thermometer, and two thermoelectric elements [16]. The thermoelectric elements kept the temperature of the sample tube 1 K colder than that of the oven.

The volume of the sample tube, the CDGs, and their connecting tubing was only 29 cm^3. A volume this small allowed the vapor to be pumped out many times before depleting the sample. Such pumping was used when zeroing the CDGs and when degassing the sample by cyclic pumping.

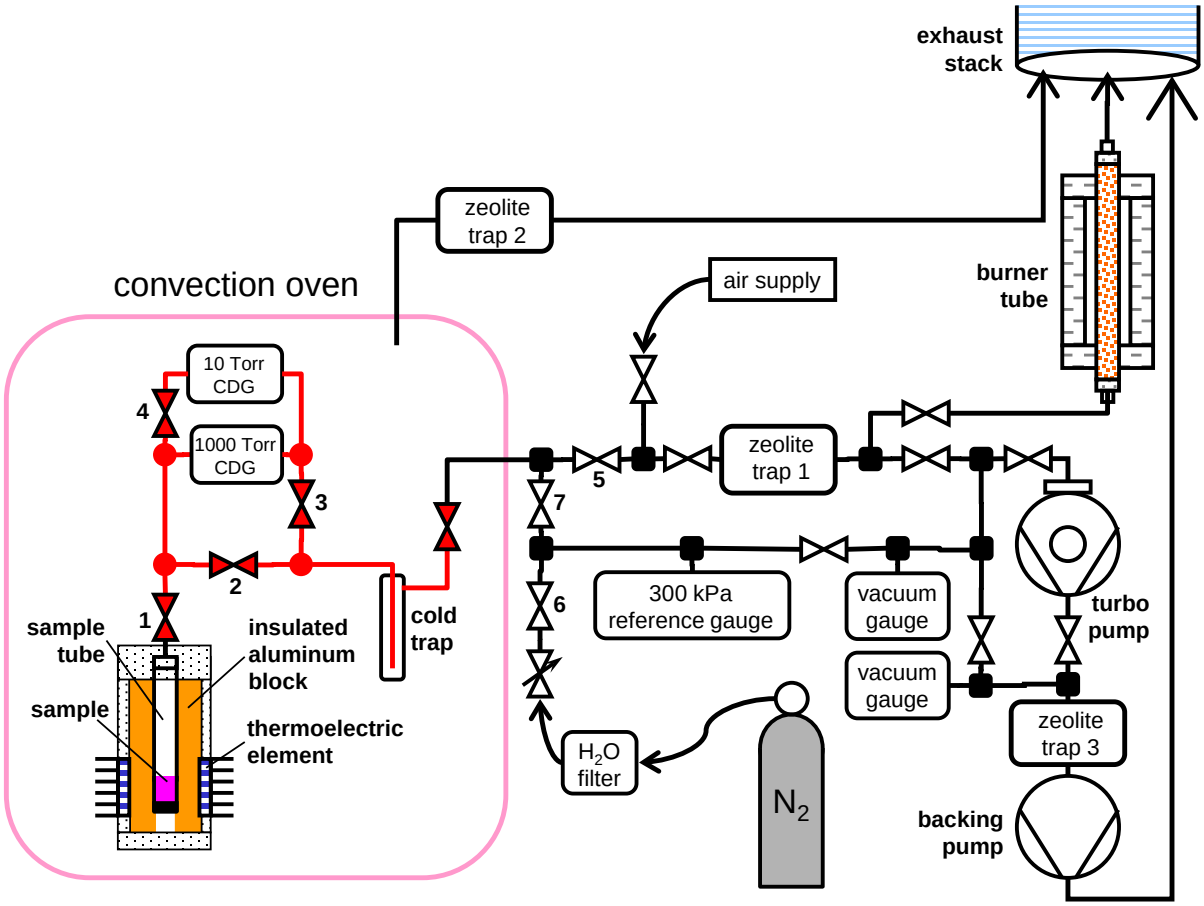

Figure 2. Apparatus schematic. (1 Torr = 133 Pa)

The sample tube was constructed by welding an end cap and a VCR fitting onto a thin-walled stainless steel tube. Because the wall thickness was only 0.07 mm, the sample temperature was

well controlled by the thermoelectric block and variations of the oven's air temperature had a negligible effect.

There were three layers of temperature control. The first layer was the laboratory room temperature, which was controlled to a precision of 0.2 K. Large variations of room temperature or humidity had little effect on the sample temperature, but they did perturb the CDG electronics. The second layer was the oven (Memmert UFE-500 [18]), which had a volume of 53 L and could be controlled up to 100 °C with a precision of 0.1 K, and at higher temperatures with a precision of 0.5 K. The third layer was the thermoelectric block that surrounded the sample tube. This device operated at temperatures as high as 200 °C while controlling the sample with a precision of 0.02 K; below 110 °C the precision was 0.002 K. Table 1 summarizes the layers of temperature control.

Table 1. The three layers of temperature control and the resulting standard uncertainty (k = 1) and stability of the sample temperature [16].

		typical	uncertainty	stability
1	Laboratory	23 °C	0.15 K	0.20 K
2	Convection oven	70	0.25	0.10
3	Thermoelectric block	69	0.006	0.002
	Sample tube	69	0.009	0.002

The CDGs (MKS model 616 [18]) were differential pressure gauges with ranges of 1.3 kPa and 130 kPa. They were designed for operation at temperatures as high as 300 °C.
The pneumatic valves (Fujikin FWB(R)-71-6.35-2 [18]) were all-metal diaphragm valves designed to operate at temperatures as high as 300 °C. The cold trap was the tube-in-tube design indicated in Figure 2; during purification it was immersed in a small coolant bath.

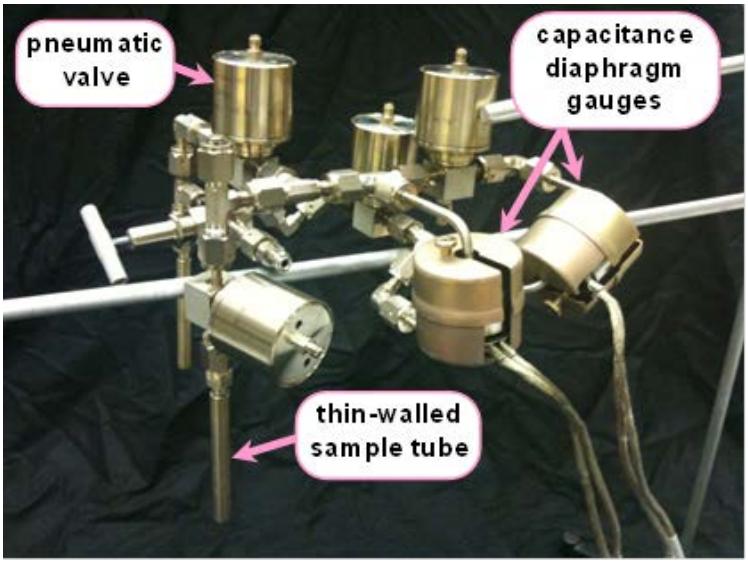

Figure 3. Photograph of the hot manifold, which comprised five valves, two CDGs, a thin-walled sample tube, and a cold trap, all of which were connected by metal gasket fittings.

2.2 Room temperature manifold

The room temperature manifold included pressure gauges, gas connections, and a 56 L s^{-1} turbo-drag pump backed by an oil-sealed rough pump. Zeolite-filled traps prevented pump oil vapor and sample vapor from reaching the turbo pump. A burner tube was used intermittently to destroy the trapped sample vapor. The burner tube was a stainless steel tube filled with copper wool and capped by a ceramic wool filters. An oven with ceramic fiber insulation surrounded the burner tube.

The quartz flexure reference pressure gauge had a full scale of 310 kPa, a resolution of 1 Pa, and a long-term stability of 31 Pa. I calibrated it against a vacuum-referenced piston gauge over the range from 2 kPa to 208 kPa, and I extrapolated the calibration to pressures below 2 kPa by assuming that the gauge's reading was a linear function of pressure. This assumption was verified by a plotting the CDG reading as a function of the quartz gauge reading; the deviations from a linear fit were smaller than 1 mPa.

3. Preparing the apparatus

3.1 Baking to remove hydrogen

Volatile impurities adsorbed onto the walls of the apparatus were removed by baking the evacuated apparatus for 1 day at 200 °C. Afterwards, dP/dt measured in the empty apparatus was dominated by hydrogen outgassing, which occurs because all stainless steel components contain dissolved hydrogen [19,20]. It is not a concern when measuring pressures above 1 Pa at temperatures below 100 °C, but at 200 °C I observed hydrogen outgassing that caused the pressure to rise as rapidly as 8 mPa s^{-1}. To reduce that outgassing, the hot manifold was pumped and baked for at least one week at temperatures from 200 °C to 250 °C. A common procedure for degassing hydrogen is to bake the vacuum chamber at 400 °C for one day [19,20], but that temperature was too high for the valves and CDGs used here.

Figure 4 shows the hydrogen outgassing that was typical for baking at 250 °C. The hot manifold without the sample tube was pumped for 12 h, and then the outgassing rate was measured by closing the valve to the pump and allowing hydrogen to accumulate for the next 12 h. Repeating this cycle for 7 days reduced the outgassing rate to approximately 0.01 mPa s^{-1} at 250 °C; the outgassing at 200 °C was 10 times smaller. Adding the empty sample tube, which was made from type 304 drawn stainless steel, caused much larger outgassing. A model based on the manifold materials and geometry (P_{calc}) indicated that the initial concentration of atomic hydrogen in the sample tube was 22 mol m^{-3}. In contrast, the initial concentration in the remainder of the manifold, which was made of type 316 vacuum remelted stainless steel, was 100 times smaller [21].

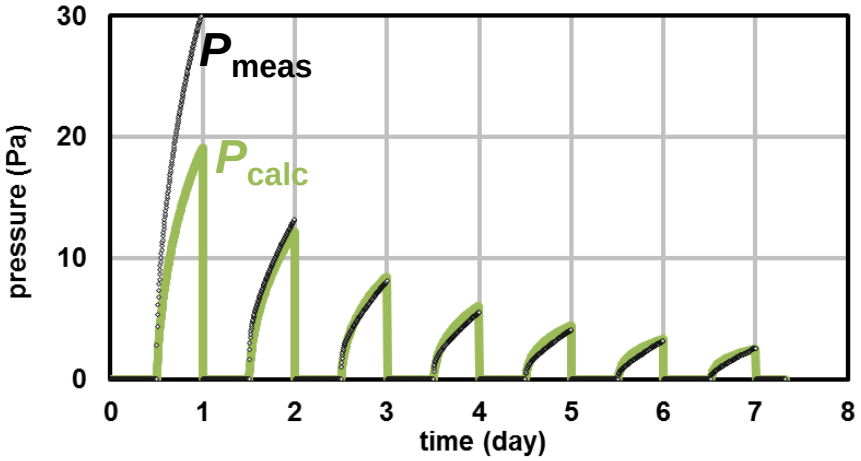

Figure 4. Baking the hot manifold at 250 °C for seven days slowly reduced the rate of hydrogen outgassing. The pressure was measured while the manifold was cyclically evacuated for 12 hours and then closed for 12 hours to allow hydrogen to accumulate in the manifold. The calculated pressure P_{calc} is discussed elsewhere [21].

The hydrogen outgassing measurements and the model are discussed in a separate article [21]. Its chief results are:

- The hydrogen outgassing rate is controlled by the geometry of the vacuum chamber's components, the hydrogen dissolved in those components, and the processes of diffusion, recombination, and trapping.
- Strongly bound or "trapped" hydrogen, which occurs at heterogeneities such as dislocations and grain boundaries, can hold most of the dissolved hydrogen even though those locations comprise fewer than 0.1 % of all lattice sites.
- The amount of hydrogen initially present in a stainless steel component can vary by a factor of 100.
- Baking at 250 °C for as long as two weeks may be necessary.

3.2 Calibrating the pressure gauges

The CDGs were calibrated by comparing them to the reference pressure gauge. There were two types of calibration. A complete calibration was done after baking the empty hot manifold, which included the CDGs, and shorter "real-time" calibrations were done during the vapor pressure measurements. In the complete calibrations, nitrogen was used to vary the pressure from zero to full scale at a series of temperatures T, and the resulting difference between the true pressure P and the nominal pressure P_{nom} was expressed as a cubic function of P_{nom},

$$P - P_{nom} = k_{p0}(T) + k_{p1}(T) P_{nom} + k_2(T) P_{nom}^2 + k_{p3}(T) P_{nom}^3 , \quad (1)$$

where the temperature dependence of each pressure coefficient was expressed as a quadratic function of T. Figure 5 shows the typical variations of the linear coefficient between complete calibrations.

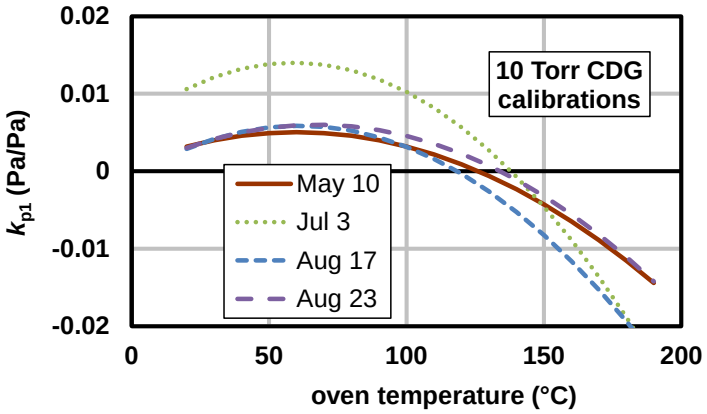

Figure 5. Typical variations of the linear pressure coefficient $k_{p1}(T)$.

The drift of the linear coefficient between calibrations could lead to an error as large as 1 %. Such errors were avoided during normal operation by performing the real-time measurements of k_{p0} and k_{p1} at each temperature, giving the true pressure

$$P = \frac{\left(P_{\text{nom}} - k_{p0}\right)}{k_{p1}}, \tag{2}$$

where P_{nom} was based on the most recent full calibration. The standard uncertainty of P combined the Type A (statistical) uncertainties of P_{nom}, k_{p0}, and k_{p1} with the Type B uncertainty $u_{\text{B}}(\text{d}P/\text{d}P_{\text{ref}})$ of the reference gauge as follows:

$$u(P) = \left[\left[u_{\text{A}}\left(k_{p0}\right)\right]^2 + \left[u_{\text{A}}\left(k_{p1}\right)\right]^2 P^2 + \left[u_{\text{A}}\left(P_{\text{nom}}\right)\right]^2 + \left[u_{\text{B}}\left(\text{d}P / \text{d}\,P_{\text{ref}}\right)\right]^2 P^2\right]^{1/2}. \tag{3}$$

The last term was negligible because $u_{\text{B}}(\text{d}P/\text{d}P_{\text{ref}}) = 0.0001$. Figure 6 shows values of $u(P)$ obtained for diethyl phthalate, ferrocene, and naphthalene during eight runs. The curves approximately describe the standard uncertainties as linear functions of pressure:

$$u(P) = \begin{Bmatrix} 0.0005P + 0.01\ \text{Pa} & \text{10 Torr CDG} \\ 0.0005P + 1\ \text{Pa} & \text{1000 Torr CDG} \end{Bmatrix}. \tag{4}$$

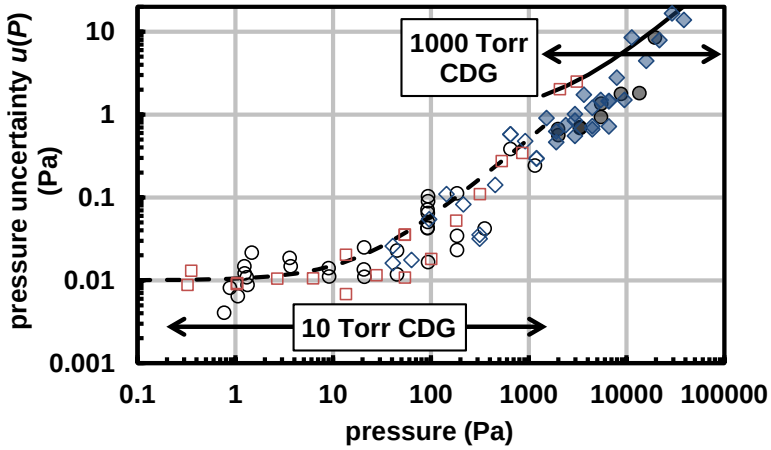

Figure 6. Standard uncertainties of the pressure measurements for diethyl phthalate □, ferrocene ○, and naphthalene ◇. The curves depict Eq. (4).

3.3 Correcting for hydrostatic head and thermal transpiration

The difference in height between the pressure gauge and the sample, Δz = 0.2 m, caused a "hydrostatic" pressure difference ΔP_z given by

$$\frac{\Delta P_z}{P} = \frac{Mg\Delta z}{RT}, \tag{5}$$

where M is the molecular mass of the vapor, g is the acceleration of gravity, and R is the universal gas constant. This correction was negligible; for TEMAH it was only 0.03 %.

The difference between the temperatures of the pressure gauge and the sample, ΔT = 1 K, caused another pressure difference ΔP_T due to thermal transpiration. Šetina [22] described the difference by

$$\frac{\Delta P_T}{P} = \frac{\left(1+\Delta T / T\right)^{1/2} - 1}{1+ f\left(Kn\right)}, \tag{6}$$

where $f(Kn)$ is a function that goes to 0 when the Knudsen number $Kn \to \infty$, namely when $P \to 0$. At T = 300 K, the transpiration corrections for Kn = 1 and $Kn = \infty$ were respectively $\Delta P_T/P$ = 0.11 % and 0.17 % and therefore negligible. This correction was small because ΔT was small and Kn = 1 occurred only at P < 1 Pa. In contrast, if the pressure gauge had been held at the constant temperature of 200 °C, the correction at Kn = 1 would have been as large as 16 %.

3.4 Loading the sample

A glove box filled with dry nitrogen (<10^{-5} mole fraction H_2O) was used to load each sample into the sample tube. Before removing the sample tube from the glove box, it was sealed by attaching pneumatic valve #1 (Figure 2). The sample tube and valve were then attached to the manifold, and the sample was degassed *in situ* by cyclic pumping, vacuum sublimation, or both methods.

4. Operation

4.1 Degassing the sample

This section describes the two methods that were used to degas the samples *in situ*, cyclic pumping and vacuum sublimation. The Appendix reviews degassing methods used elsewhere.

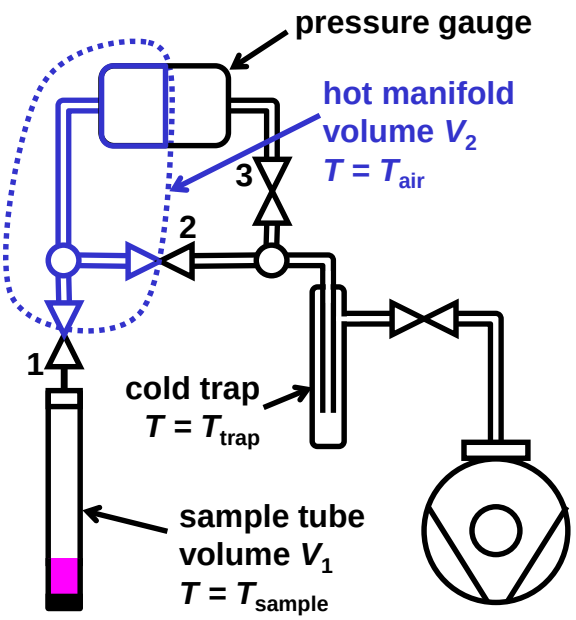

Figure 7. Components used for degassing and cyclic pumping.

4.1.1 Degassing by cyclic pumping

See Figure 7. Cyclic pumping periodically removed a known volume of vapor from the sample. It comprised as many as 100 repetitions of the following cycle:

1. Isolate the sample tube. (Close valve 1.)
2. Pump the vapor out of the hot manifold. (Open valve 2 to the hot manifold.)
3. Stop pumping and open the sample tube to the hot manifold. (Close valve 2 and open valve 1.)

Degassing by cyclic pumping has the following advantages:

- The amount of sample removed per cycle is known even if the sample is in an opaque container, as described below.
- The amount of sample removed is small if the sample vapor pressure and the manifold volume are small.
- The cycle time can be adjusted to allow for the impurity's speed of diffusion into the vapor.
- It is easily automated.

Assuming that the sample is a binary solution that consists almost entirely of compound "A", the moles of A removed during a pumping cycle is:

$$\Delta n_{VA} = \frac{V_2 P_{VA}}{RT}, \tag{7}$$

where P_{VA} is the vapor pressure of A. The amount of impurity "B" removed during the same cycle is proportional to the mole fraction y_B of B in the vapor. Assuming Raoult's law, y_B is given by

$$P y_B = k_H x_B \cong P_{VB} x_B, \tag{8}$$

where P is the total pressure, x_B is the molar concentration of B in the liquid (or solid), k_H is Henry's constant, and P_{VB} is the vapor pressure of B. The moles of impurity "B" removed during cycle "i" is then

$$\Delta n_{VB}(i) = \frac{V_2 P_{VB} x_B(i)}{RT} = \alpha x_B(i) \Delta n_{VA}. \tag{9}$$

Here, α is volatility ratio defined by

$$\alpha = \frac{y_B / x_B}{y_A / x_A} \cong \frac{k_H / P_{VA}}{1/1} \approx \frac{P_{VB}}{P_{VA}}, \tag{10}$$

The impurity decrease per cycle $\Delta x(i)$ is then given by

$$\frac{\Delta x_B(i)}{x_B(i)} \cong (\alpha - 1)\frac{\Delta n_{VA}}{n_{LA}} \approx \frac{(P_{VB} - P_{VA})V_2}{n_{LA}RT}, \tag{11}$$

where n_{LA} is the amount of compound A in liquid form. Equation (11) says that the impurity decrease is proportional to α - 1, so little improvement is possible when the impurity has a vapor pressure similar to that of compound A. Rewriting Eq. (11) as a differential equation and integrating yields the Rayleigh distillation equation, Eq. (29) in the Appendix.

Figure 8 illustrates the degassing of diethyl phthalate by cyclic pumping. Possible impurities included nitrogen and maleic anhydride. The sample was held at T_{sample} = 99 °C, and the cycle comprised a 15 min evacuation of the hot manifold followed by a 15 min observation of the increasing pressure. After 17 h, the rate of pressure increase was less than 0.3 Pa h^{-1}.

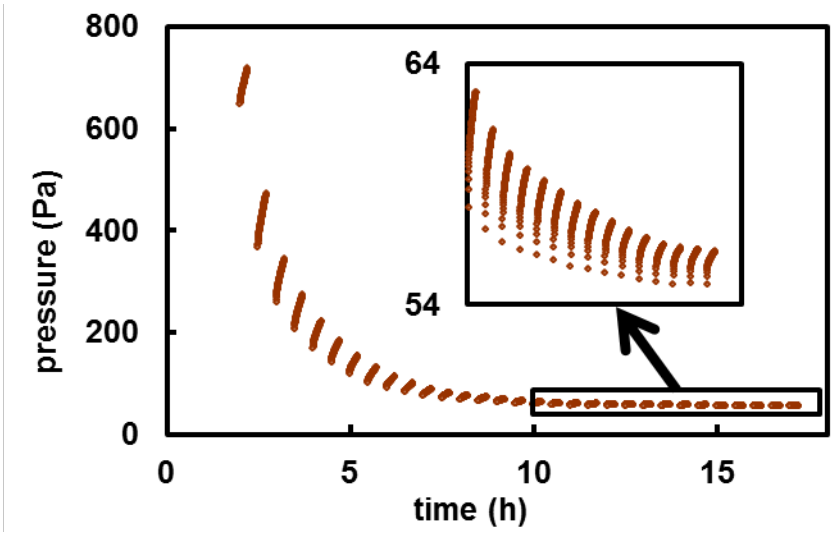

Figure 8. Partial degassing of diethyl phthalate by cyclic pumping at 99 °C. The cycle comprised a 15 min evacuation of the hot manifold followed by a 15 min observation of the increasing pressure. After 17 h, the rate of pressure increase was less than 0.3 Pa h^{-1}.

The sample was then degassed further at temperatures as high as 159 °C. Figure 9 shows subsequent measurements of vapor pressure at 99 °C. Following an evacuation and the short recovery from evaporative cooling, the pressure increased at less than 0.02 Pa h^{-1}, which was similar to the expected rate of hydrogen outgassing [21].

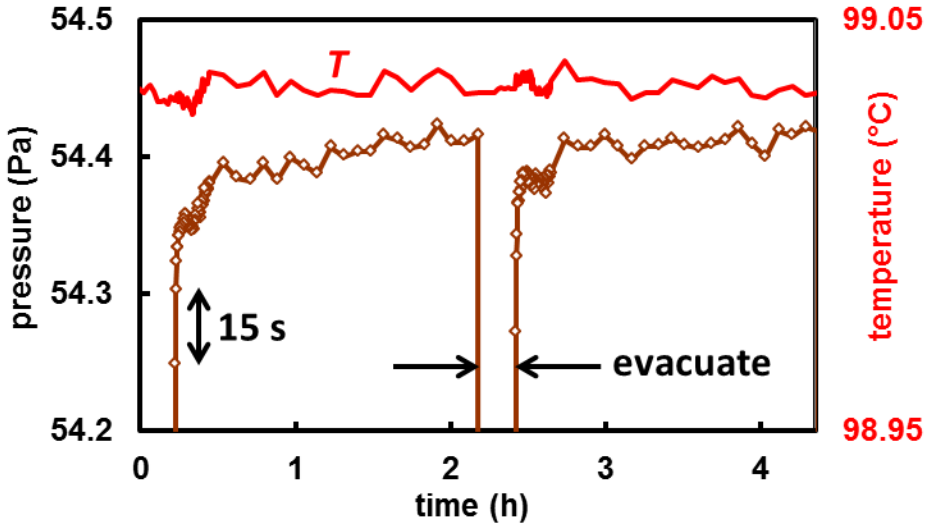

Figure 9. Typical measurements of diethyl phthalate after degassing by cyclic pumping at 99 °C and 159 °C. Following the recovery from evaporative cooling, the pressure increased at less than 0.02 Pa h^{-1}.

Stirring the diethyl phthalate was tried in one run at 99 °C. The stirrer was a stainless steel ball bearing inside the sample tube that was periodically lifted and dropped by an external magnet attached to a gearhead motor. Stirring caused only a small improvement of the degassing, perhaps because boiling was already stirring the sample [17].

4.1.2 Degassing by vacuum sublimation

Cyclic pumping may not be effective if the impurity has a small diffusivity, which is more likely when the sample is solid. For example, the self diffusivity of polycrystalline naphthalene near its melting point of 80 °C ($D = 1\times10^{-9}$ m^2s^{-1} [23]) is similar to that of the liquid (Wilke-Chang method [24,25]). However, at 40 °C, it is about 40 times smaller, and the diffusion time of a 10 mm deep sample is approximately 18 days.

In contrast, vacuum sublimation works for solids as well as liquids [5]. It is a variation of batch distillation that is performed at pressures below atmospheric. See, for example, [26]. The sample is evaporated in vacuum at temperature T_{sample} and condensed into a cold trap at $T_{trap} < T_{sample}$. Scientific laboratories typically use this method to remove an impurity of lower volatility, which remains behind in the sample container. However, when the impurity has a higher volatility, the entire sample is evaporated with the expectation that the impurity will be more likely to pass through the trap to the vacuum pump.

The following steps were used:

1. Remove gas at atmospheric pressure: Freeze the sample in the sample tube at 77 K, open the vacuum pump, pump out all gas from above the sample, then close the sample tube and warm it to T_{sample}.

2. Cool the cold trap to T_{trap}, typically 77 K or 273 K, and open the sample tube to condense the sample into the trap. A warm value of T_{trap} will allow an impurity of moderate volatility to pass through the trap, but it also will cause more of the sample to be lost to the pump.
3. Close the vacuum pump, warm the trap to T_{air}, cool the sample tube to 77 K, and then condense the sample back into the sample tube.

The efficiency of this method depends on T_{sample}, which controls the rate of evaporation, T_{air}, which controls the sticking coefficient on the wall of the connecting manifold, and T_{trap}, which controls the relative amounts of sample and impurity that pass through the trap to the vacuum pump.

The CDG pressure reading allowed the progress of the sublimation to be followed even though the sample could not be seen inside the metal manifold. The pressure reading was always time dependent and smaller than the vapor pressure at T_{sample}. Its value was likely determined by the flow conductance of the hot manifold and the flow rate through the manifold.

The simple, all-metal, tube-in-tube design used here was adequate, but more elaborate geometries are possible, such as the use of two intermediate traps by Pangrác et al. [15]. One might also replace the intermediate traps by a long tube that functioned as a preparative chromatograph. An attempt with a long coiled tube failed because condensate clogged the bottom of the first coil.

4.2 Measuring $P_V(T)$

The apparatus was driven by a sequence of commands listed in a spreadsheet and implemented by the spreadsheet's scripting language. Figure 10 shows a measurement run in which the temperature was increased in 10 K steps. At each temperature two or more pumping cycles removed vapor, and a limited "real-time" calibration obtained the parameters k_{p0} and k_{p1} for both CDGs.

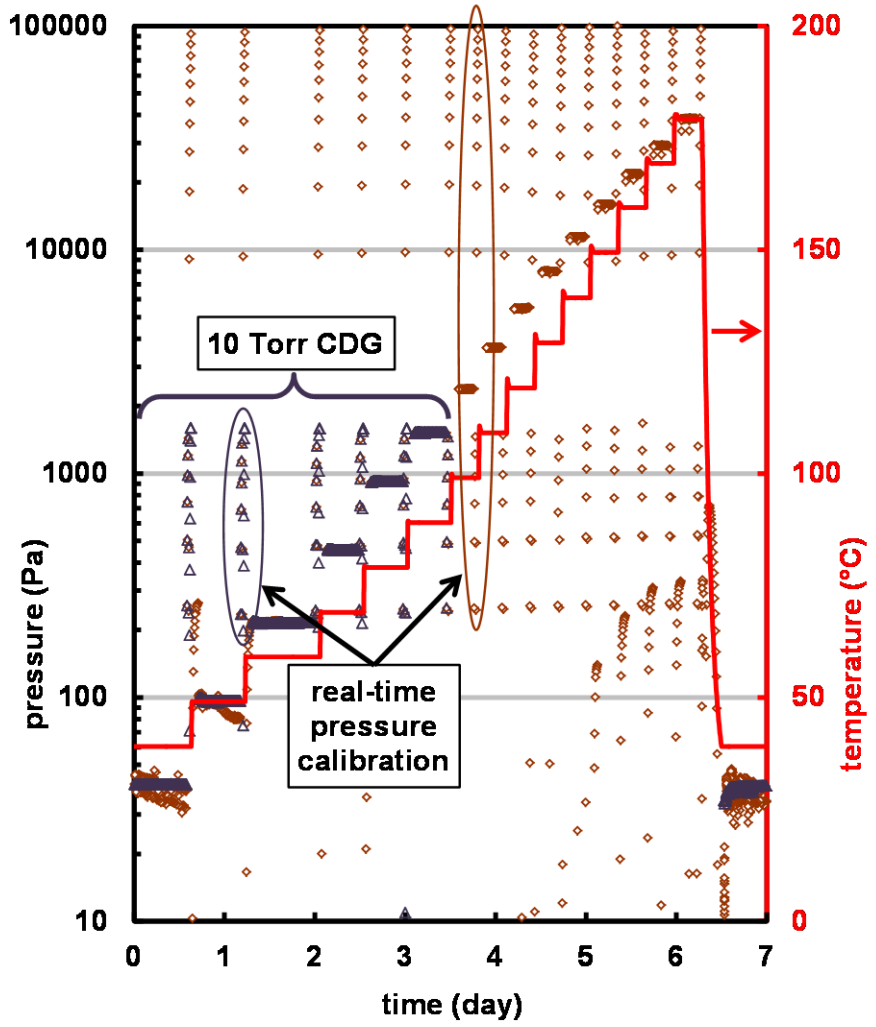

Figure 10. A typical measurement run. The dense horizontal groups of points are the vapor pressure of the naphthalene sample, and the sparse vertical groups are the pressure of nitrogen gas that was used for a "real-time" pressure calibration at each temperature.

Figure 11 shows details of the measurements. At 169 °C, where the sample was liquid, the pressure returned quickly to equilibrium after an evacuation, and subsequent variations were driven by small variations of the sample temperature. At 59 °C, where the sample was solid, the pressure equilibrated slowly.

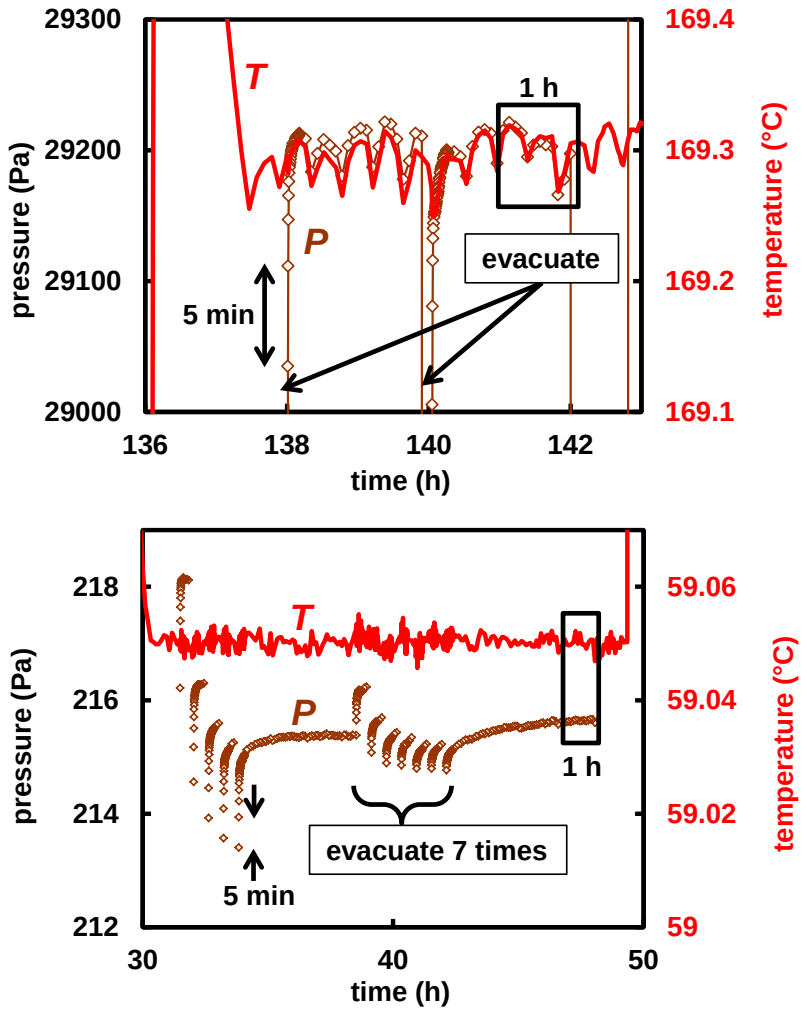

Figure 11. Details of Figure 10. At 169 °C (upper), the naphthalene sample was liquid, and the pressure returned quickly to equilibrium after an evacuation. Subsequent variations of pressure were driven by small variations of the sample temperature. At 59 °C (lower), the sample was solid, and the pressure equilibrated slowly. The vapor pressure was obtained by averaging the data in the indicated 1 h intervals.

4.3 Response times

The speed of the vapor pressure measurements was limited by the slow responses of the apparatus and the sample. The slowest apparatus components were the CDGs, which required 2 h to stabilize after a change of 20 K. This long interval may have been due to the slow relaxation of mechanical stress. Although CDG manufacturers typically do not specify the relaxation time

of their devices, variation among models is possible; the relaxation time for a CDG made by another manufacturer was observed to be almost 4 h.

The sample's response can be even slower due to the diffusion of a volatile impurity out of the condensed sample. Pumping on the sample reduces the impurity concentration at the sample surface and creates a concentration gradient within the sample. If the sample is a solid or an unstirred liquid, the gradient will relax with the characteristic time

$$\tau_D = \frac{L^2}{\pi^2 D}, \tag{12}$$

where L is the sample's effective diffusion length and D is the mass diffusion constant. Table 2 gives example values of D and τ_D for various liquid mixtures. See the companion article [17] for details.

Table 2. Estimates of the mass diffusion constant D and concentration relaxation time $\tau_D = L^2/(\pi^2 D)$ in a liquid sample of thickness L = 10 mm at 80 °C [17].

liquid A	impurity B	P_{VB} / P_{VA}	D (10^{-9} m^{2}s^{-1})	τ_D (h)
naphthalene	nitrogen	3.6×10^5	3.6	0.8
diethyl phthalate	nitrogen	2.5×10^7	0.23	12
diethyl phthalate	maleic anhydride	8.9×10^1	0.16	18
TEMAH	methyl ethylamine	2.4×10^3	0.37	8

The sample's time constant for thermal equilibration was expected to be only about 100 s [17]. However, that estimate, which assumed good contact with the container wall, may have been too small for a solid sample. Pumping on the sample preferentially evaporates the warm layer close to the wall, and the resulting gap has a low thermal conductance.

Another slow process is redistribution of the sample when the temperature of the sample container has a nonuniformity ΔT_0. As discussed in [17], transpiration will cause the difference between the measured pressure P and the vapor pressure $P_V(T_0)$ at the container's nominal temperature T_0 to be approximately

$$P - P_V(T_0) \simeq \frac{dP_V}{dT}\Delta T_0 . \tag{13}$$

Depending on the sample's distribution in the container, the pressure difference can persist for hours.

4.4 Trapping vapor

During the measurements, zeolite trap #1 captured the vapor produced by degassing the sample and zeroing the CDGs. Afterwards, the trapped vapor was destroyed by warming the zeolite trap to 150 °C, heating the burner tube to 700 °C, and flowing air through the trap to drive the vapor into the burner tube. The vapor was oxidized to metal oxides and gases such as H_2O and CO_2. The oxides were trapped by the ceramic wool filter pad at the end of the burner tube, and the gases were exhausted outside the building.

The zeolite trap was safer than a cryogenic trap because it required less attention. Any water already present in the zeolite enhanced the trap's safety by promoting the oxidation of the vapor in the trap. Using only a small sample, typically 1 cm^3, minimized the concerns of safety and disposal. Although this trap-and-burn scheme was suitable only for small amounts of vapor, it could handle a wide variety of compounds, which is useful for a scientific laboratory; see, for example, [15]. In contrast, the scheme used by a semiconductor fab can mitigate a large amount of vapor, but it must be optimized for a particular process chemistry.

5. Results

Figure 12 uses data for four compounds to show the range of data collected with the present apparatus. For naphthalene, ferrocene, and diethyl phthalate the vapor pressure P_v was defined to be the pressure measured when the condensed sample was in approximate equilibrium with its vapor. This occurred after the sample temperature had recovered from evaporative cooling, as discussed in [17], and before a significant amount of impurity had diffused out of the sample into the vapor. The P_v values for these three compounds are tabulated in Section 5.2. The results for TEMAH, which were affected by decomposition, are discussed in a separate section.

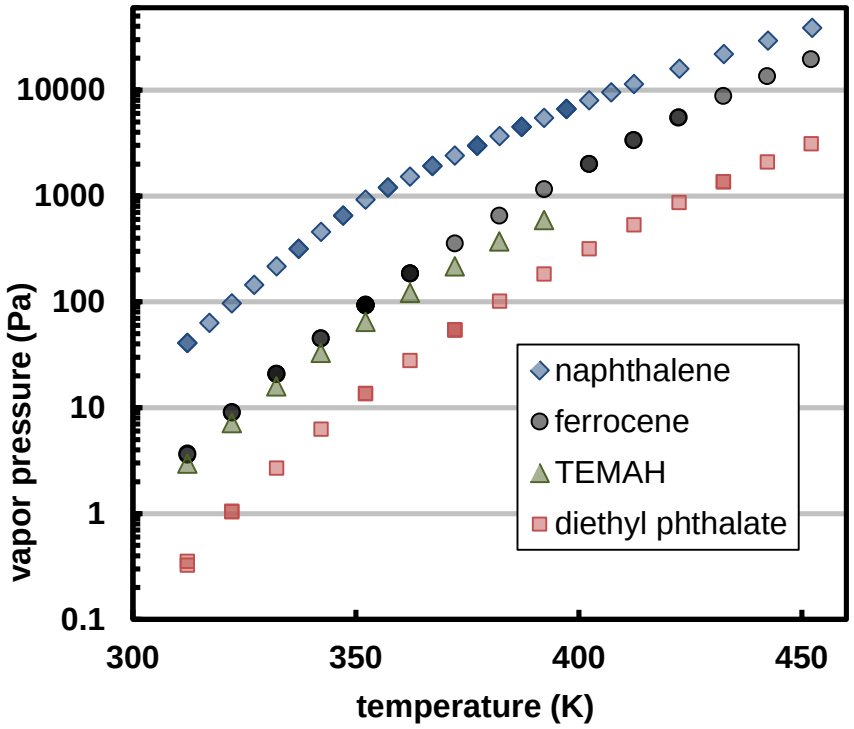

Figure 12. Data collected with the present apparatus.

5.1 Purity

Table 3 lists the as-received purities of the compounds and the methods used to purify the samples further *in situ*. As discussed in the companion article [17], an impurity B with mole

fraction x_B in the sample and partial pressure P_B in the vapor will cause a relative error of approximately

$$\frac{P_B}{P_{VA}} \simeq x_B \left(\frac{P_{VB}}{P_{VA}} - 1 \right), \tag{14}$$

where P_{VB} and P_{VA} are the vapor pressures of the impurity and the pure compound. The error depends very much on the impurity, and one with a vapor pressure similar to P_{VA} will have little effect. In contrast, dissolving only 3×10^{-6} mole fraction of nitrogen in naphthalene at 80 °C will double the observed pressure.

Table 3. The as-received purity and the method used to purify the samples further *in situ*.

chemical name CAS	source	initial mole fraction purity	purification method	final mole fraction purity	analysis method
naphthalene [a] 91-20-3	Sigma Aldrich	0.997	vacuum sublimation	[e] $P_B/P_{VA} < 0.05$	Eq. (15)
ferrocene [b] 102-54-5	Aldrich	0.998	vacuum sublimation	[e] $P_B/P_{VA} < 0.05$	Eq. (15)
diethyl phthalate [c] 84-66-2	Sigma Aldrich	0.995	cyclic pumping	[e] $P_B/P_{VA} < 0.05$	Eq. (15)
TEMAH [d] 352535-01-4	SAFC Hitech	0.990	cyclic pumping	[f] $0.03 < P_B/P_{VA} < 0.18$	Eq. (18)

[a] bicyclo[4.4.0]deca-1,3,5,7,9-pentene
[b] bis(η^5-cyclopentadienyl)iron
[c] diethyl benzene-1,2-dicarboxylate
[d] tetrakis(ethylmethylamino)hafnium
[e] Bound on P_B/P_{VA} obtained from Eq. (15).
[f] Range of P_B/P_{VA} obtained from fits to Eq. (18).

A bound on the impurity concentration in the vapor (not the condensed sample) can be obtained from the time dependence of the pressure $P(t)$ observed after pumping on the sample. At the time $t = 0.01\,\tau_D$, where τ_D is the time constant for mass diffusion, the partial pressure of the impurity P_B will be given approximately by [17]

$$\frac{P_B(t)}{P_{VA}} \approx \left(\frac{1}{P} \frac{dP}{dt} \right) \tau_D . \tag{15}$$

For the first three compounds, the *in situ* purification typically reduced the pressure time dependence to below the measurement resolution of $(dP/dt)/P \approx 10^{-6}$ s^{-1}. For the typical time of τ_D = 14 h [17], the corresponding bound on the impurity concentration in the vapor is 0.05.

For TEMAH, which decomposed continuously, the time dependence of the pressure was always large. As described in [17] and later in this article, fitting Eq. (18) to $P(t)$ obtained the desired vapor pressure even when $P_B/P_{VA} > 1$.

5.2 Naphthalene, ferrocene, and diethyl phthalate

Figure 13 shows that the scatter ΔP_V among the values of P_V was often larger than the pressure uncertainty $u(P)$. The scatter was estimated by subtracting P_V from a reference function P_{Vref}, and then calculating the standard deviations of P_V - P_{Vref} three points at a time.

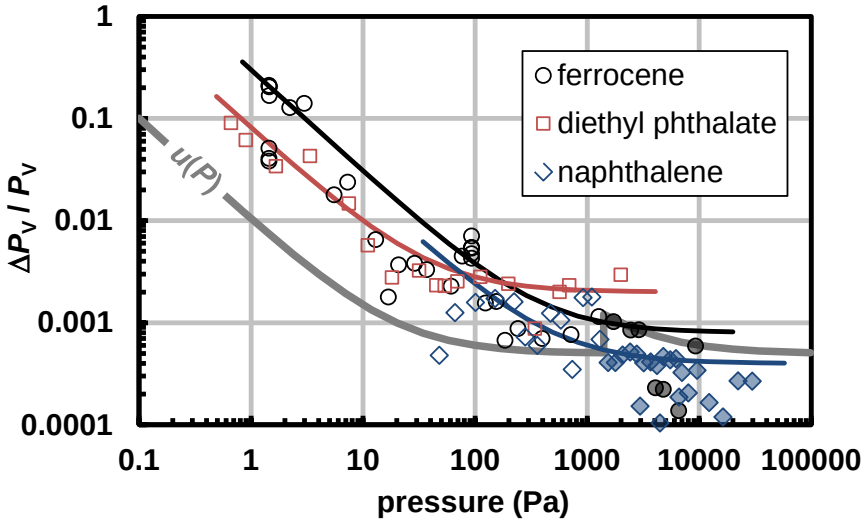

Figure 13. The measured scatter ΔP_V was often larger than the pressure uncertainty $u(P)$. The three upper curves are approximate descriptions of ΔP_V.

At low pressure ΔP_V varied with the compound and was as much as 50 times larger than $u(P)$. The curves on Figure 13 approximately describe ΔP_V as follows.

$$\frac{\Delta P_V}{P_V} = \left\{ \begin{array}{ll} 0.0004 + (0.2\ \text{Pa}) / P & \text{naphthalene} \\ 0.0008 + (0.3\ \text{Pa}) / P & \text{ferrocene} \\ 0.002 + (0.08\ \text{Pa}) / P & \text{diethyl phthalate} \end{array} \right\} \tag{16}$$

The following expression describes the total relative standard uncertainty of P_V for these three compounds.

$$\frac{u(P_V)}{P_V} = \left[\left(\frac{T}{P_V} \frac{dP_V}{dT} \right)^2 \left(\frac{u(T)}{T} \right)^2 + \left(\frac{\Delta P_V}{P_V} \right)^2 \right]^{1/2} \simeq \frac{\Delta P_V}{P_V} \tag{17}$$

The first term of Eq. (17) was usually negligible because $u(T)$ = 9 mK; for example, it was 0.0006 for naphthalene near its melting temperature of 353 K. There is no term for $u(P)$ because it is implicitly included in ΔP_V.

Table 4. Vapor pressures[a] of diethyl phthalate, naphthalene, and ferrocene. The liquid phase data are separated by a dashed line and indicated in bold font.

diethyl phthalate		naphthalene		ferrocene	
T / K	P_V / Pa	T / K	P_V / Pa	T / K	P_V / Pa
312.211	0.32	312.203	40.84	312.204	3.69
312.211	0.35	312.205	40.83	312.208	3.59
322.213	1.05	317.210	63.26	322.209	9.00
322.213	1.03	322.210	96.22	322.212	9.11
332.211	2.69	327.211	144.65	332.202	20.78
342.187	6.23	332.210	215.32	332.208	20.86
352.183	13.58	337.206	315.04	332.211	20.71
352.197	13.52	337.207	315.43	342.178	44.97
362.198	27.75	342.185	455.65	342.179	45.17
372.193	54.29	347.186	651.04	352.169	93.23
372.200	54.07	347.187	650.96	352.169	92.72
372.219	54.24	352.194	921.31	352.171	93.73
382.225	100.85	**357.190**	**1200.3**	352.172	93.40
392.241	182.06	**357.191**	**1199.7**	352.176	92.49
402.368	316.85	**362.196**	**1520.7**	352.176	92.64
412.380	530.31	**367.209**	**1915.2**	352.182	93.28
422.489	862.13	**367.209**	**1913.8**	352.192	93.60
442.276	2082.3	**372.218**	**2393.5**	362.170	185.07
452.116	3098.9	**377.219**	**2966.2**	362.171	185.04
		377.221	**2966.9**	362.184	185.43
		377.223	**2966.2**	372.197	354.27
		382.220	**3656.6**	382.193	650.79
		387.227	**4474.7**	392.198	1158.2
		387.232	**4474.9**	402.264	2000.5
		387.233	**4475.8**	402.311	2008.1
		392.242	**5450.4**	412.238	3345.9
		397.269	**6592.6**	412.318	3360.6
		397.269	**6593.1**	422.287	5470.1
		397.271	**6595.6**	422.403	5501.7
		402.368	**7961.5**	432.418	8756.2
		407.325	**9502.4**	442.265	13532
		412.397	**11329**	**452.085**	**19481**
		422.548	**15876**		
		432.579	**21747**		
		442.461	**29184**		
		452.367	**38569**		

[a] $u(T) = 0.009$ K

naphthalene $u(P_V) / P_V = 0.004 + (0.2\ \text{Pa}) / P_V$

ferrocene $u(P_V) / P_V = 0.008 + (0.3\ \text{Pa}) / P_V$

diethethyl phthalate $u(P_V) / P_V = 0.02 + (0.08\ \text{Pa}) / P_V$

Naphthalene

Figure 14 compares the naphthalene results to previous measurements. Above the melting temperature T_{melt}, the values typically have standard uncertainties from 0.02 % to 0.2 %, and they agree with previous results from Camin and Rossini [24], Fowler et al. [27], and Chirico et al. [28]. At the coldest temperature of 312 K, the values fall between the values of Růžička et al. [29] and Monte et al. [13].

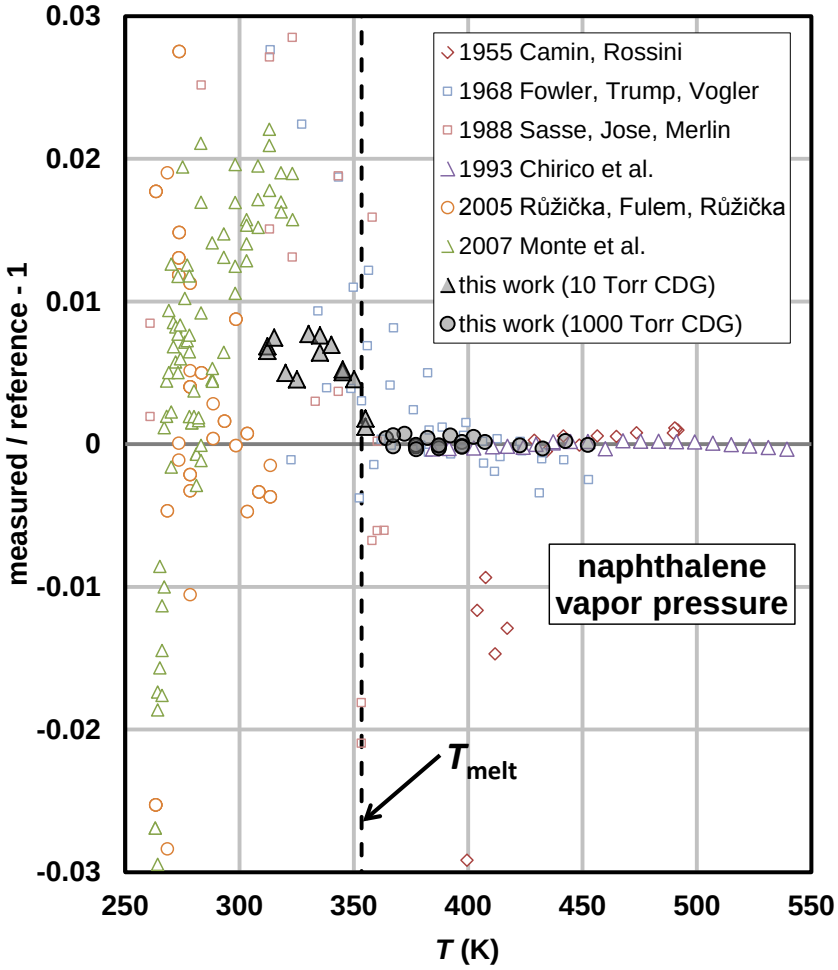

Figure 14. Naphthalene results compared to previous results from Sasse et al. [8], Monte et al. [13], Camin and Rossini [24], Fowler et al. [27], Chirico et al. [28], and Růžička et al. [29]. At the coldest temperature of 312 K, the values fall between the values of [29] and [13]. The reference function from [31] defines zero. Scatter dominated the uncertainty of the present results.

Ferrocene

Figure 15 compares present results for ferrocene from Kaplan et al. [31], Edwards and Kington [32], Emel'yanenko [33], Siddiqi [34], Monte et al. [13], and Fulem et al. [35]. Except for the two coldest points at 312 K, the present data were reported previously by Fulem et al. [35]. In that work, the authors combined calculated ideal gas heat capacities and critically assessed experimental data for vapor pressure, crystalline heat capacity, and enthalpy of sublimation to obtain a consistent thermodynamic description.

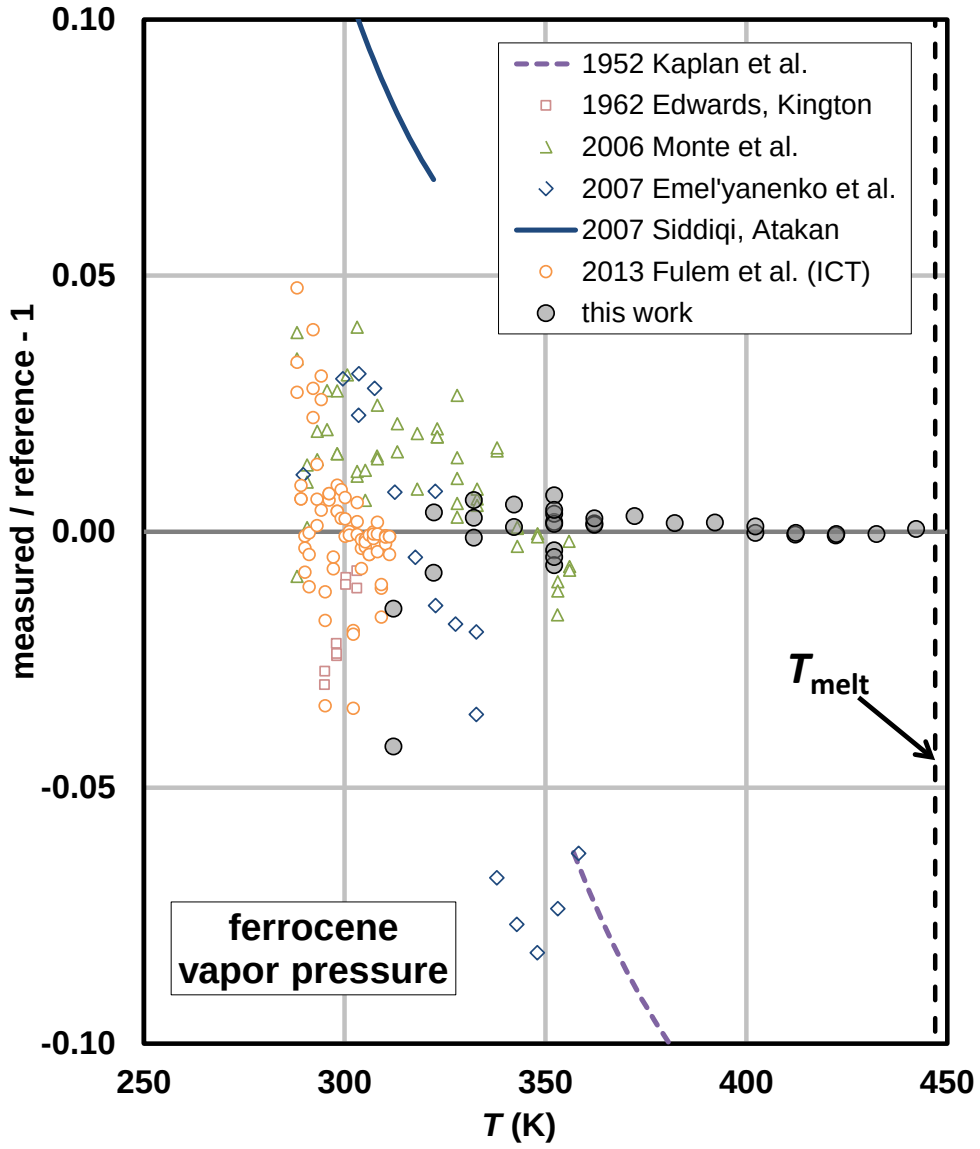

Figure 15. Ferrocene results compared to previous results from Kaplan et al. [32], Edwards and Kington [33], Monte et al. [13], Emel'yanenko et al. [34], Siddiqi and Atakan [35], and Fulem et al. [36]. Zero is defined by Eq. (3) of Fulem et al. [36]. Except for the two points at 312 K, the present data were reported previously in [36]. Scatter dominated the uncertainty of the present results.

Diethyl phthalate

Figure 16 compares the present results to previous work by Rohác et al. [37], who used three methods to span the remarkably wide temperature range of 217 K. Below 350 K, the present results disagree with those of [37] by as much as 20 %, and the Knudsen and static results from [37] disagree by about 10 %.

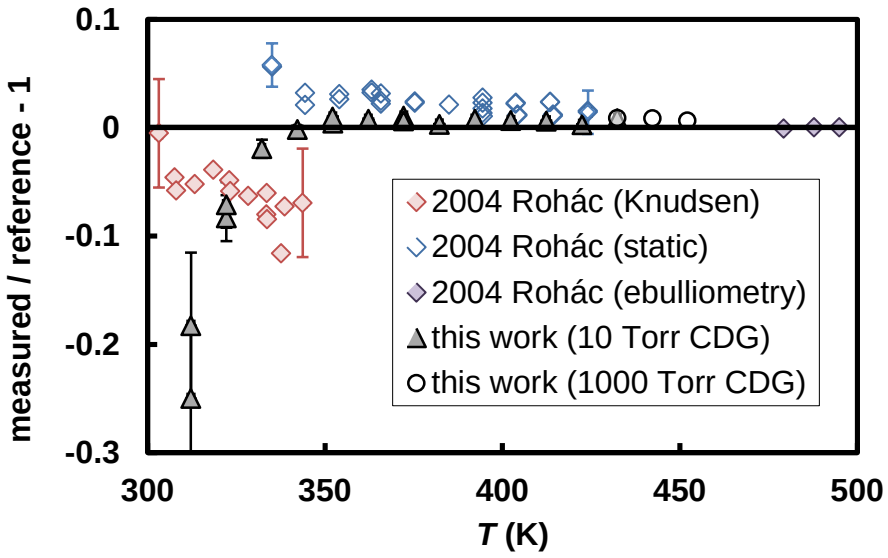

Figure 16. Diethyl phthalate results compared to the reference function, Eq. (4) of Rohác et al. [37]. The standard uncertainty of the present results is comparable to or smaller than the size of the point above 330 K, and the uncertainty of the results from [37] is indicated by error bars at selected temperatures.

6. Tetrakisethylmethylaminohafnium (TEMAH)

Decomposition complicated the vapor pressure measurements of TEMAH. Figure 17 shows examples of the time-dependent pressure observed after opening the manifold to the sample tube containing TEMAH. As discussed in the companion article [17], five processes contributed caused the time dependence:

1. Evaporative cooling at $t = 0$.
2. Temperature equilibration.
3. Generation of a volatile impurity by decomposition with reaction rate k_A.
4. Removal of the impurity with effective reaction rate k_B.
5. Diffusion of the impurity from the liquid to the vapor, characterized by the rate k_D.

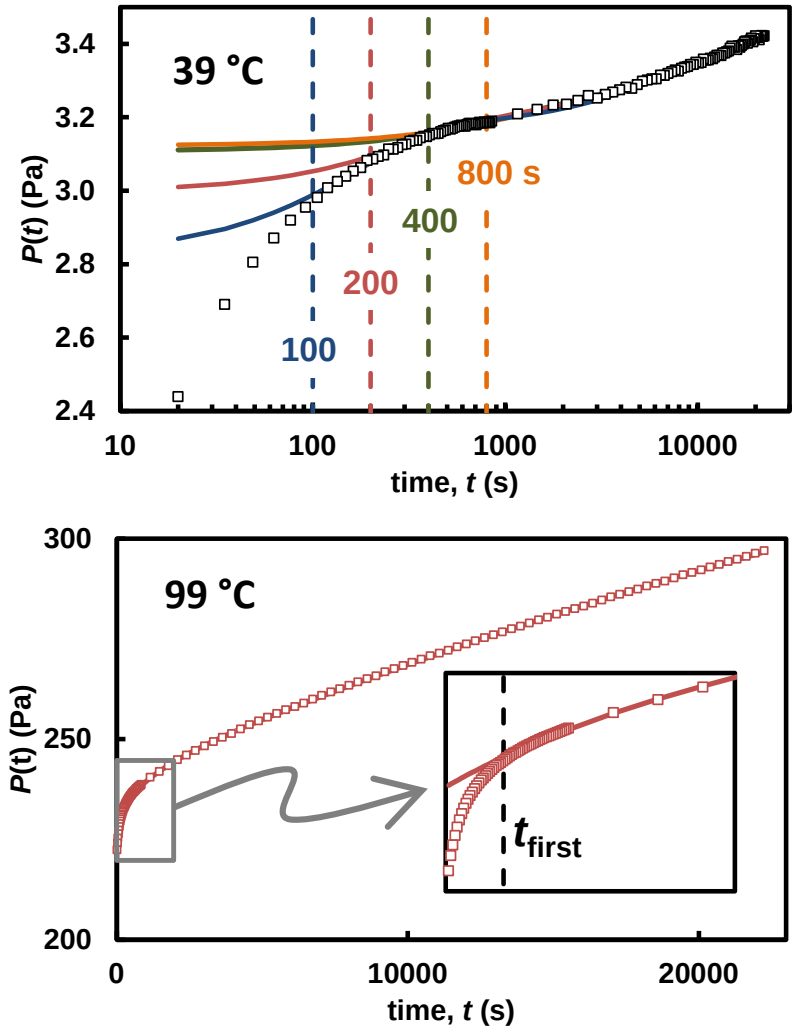

Figure 17. Decomposition of TEMAH caused the pressure to be time dependent. UPPER: At 39 °C, the decomposition rate was small and evaporative cooling was relatively large. The curves show fits of Eq. (18) with various values of t_{first}; Eq. (18) ignored temperature equilibration by fitting only to data after $t > t_{first}$. LOWER: At 99 °C, the decomposition rate was larger.

Temperature equilibration was assumed to be finished after t_{first} = 400 s, and the other processes were accounted for by the following equation, which was fitted to the data at times $t > t_{first}$:

$$P_{fit}(t) = P_{fit}(0) + P_B(\infty)\left(1 - e^{-t/\tau_B}\right) + P_1\left(\frac{1}{1+\gamma}\right)e^{-t/\tau_B}\left(1 - e^{-t/\tau_D}\right) \qquad (18)$$

Here,

$$\begin{aligned} P_{\text{fit}}(0) &= \text{fitted pressure at } t = 0 \\ P_B(\infty) &= \text{ final, equilibrium pressure of the impurity B} \\ P_1 &= \text{ disequilibrium pressure of the impurity at } t = 0 \\ \tau_B &= \text{ time constant for the removal of impurity B} \\ \tau_D &= \text{ time constant for diffusive equilibration of the impurity} \end{aligned} \tag{19}$$

and the partition parameter γ is defined by

$$\gamma \equiv \frac{(\text{moles B in vapor})}{(\text{moles B in liquid})} = \frac{M_A P_{VB}(V_1 + V_2)}{mRT}, \tag{20}$$

where m is the mass of the liquid sample, M_A is the molar mass of TEMAH, and $V_1 + V_2$ is the volume of the vapor space. The equilibrium impurity pressure is related to the reaction rates k_A and k_B by

$$P_B(\infty) = \frac{k_B}{k_A} P_{VB}, \tag{21}$$

where P_{VB} is the vapor pressure of the impurity, and the two time constants are defined by

$$\frac{1}{\tau_B} \equiv \left(\frac{\gamma}{1+\gamma}\right) k_B \quad \text{and} \quad \frac{1}{\tau_D} \equiv \left(\frac{1+\gamma}{\gamma}\right) k_D. \tag{22}$$

The five fitted parameters in Eq. (18) are the pressures $P_{\text{fit}}(0)$ and P_1 (units Pa) and the rate constants k_A, k_B, and k_D (s^{-1}). The most important is

$$P_{\text{fit}}(0) = P_{VA} + P_B(0), \tag{23}$$

which is the sum of P_{VA}, the vapor pressure of the compound of interest, and $P_B(0)$, the partial pressure of the impurity at $t = 0$.

The fitted value of $P_{\text{fit}}(0)$ had a weak dependence on the range of data. As shown in Figure 18, decreasing the time of the first fitted point from the nominal value of $t_{\text{first}} = 400$ s had the largest effect at 39 °C, probably because boiling-induced stirring was smaller at colder temperatures. Figure 17 shows that increasing t_{first} to 800 s had little effect on $P_{\text{fit}}(0)$. The value $t_{\text{first}} = 400$ s was chosen to minimize the statistical uncertainty of $P_{\text{fit}}(0)$ at all temperatures.

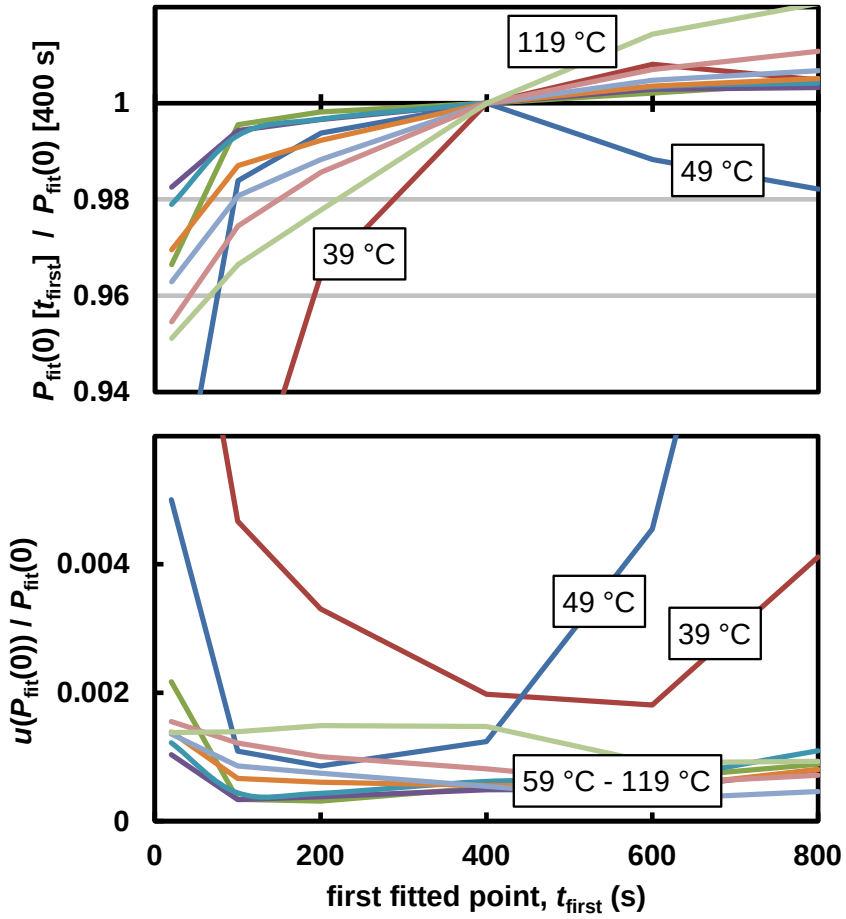

Figure 18. UPPER: The fitted value of $P_{fit}(0)$ had only a weak dependence on the range of data. Decreasing the time of the first fitted point from the nominal value of t_{first} = 400 s had the largest effect at 39 °C, probably because boiling-induced stirring was smaller at colder temperatures. LOWER: The statistical uncertainty of $P_{fit}(0)$ depended weakly on t_{first} except at 39 °C and 49 °C.

Separating P_{VA} from $P_{fit}(0)$ in Eq. (23) was possible because the measurements of $P(t)$ were preceded by cyclic pumping, which added an additional constraint. Figure 19 shows the periodic variations of $P(t)$ that preceded a 6 h measurement: At $t = 0$ the sample tube (volume V_1) was opened to the total manifold volume ($V_1 + V_2$). At $t = t_1$, the sample tube was closed while the rest of the manifold was evacuated. During that second interval, decomposition continued to increase the pressure in the sample tube. As explained in [17], extrapolating the fitted pressure $P_{fit}(t)$ to the time t_2 allowed P_{VA} to be estimated as:

$$P_{VA} = \frac{P_{fit}(0)}{(1-V_{12})} + P_{fit}(t_1) - \frac{P_{fit}(t_2)}{(1-V_{12})}, \qquad (24)$$

where the volume ratio is $V_{12} \equiv V_1 / (V_1 + V_2)$. Expansion of nitrogen gas from V_1 to $(V_1 + V_2)$ was used to measure V_{12}.

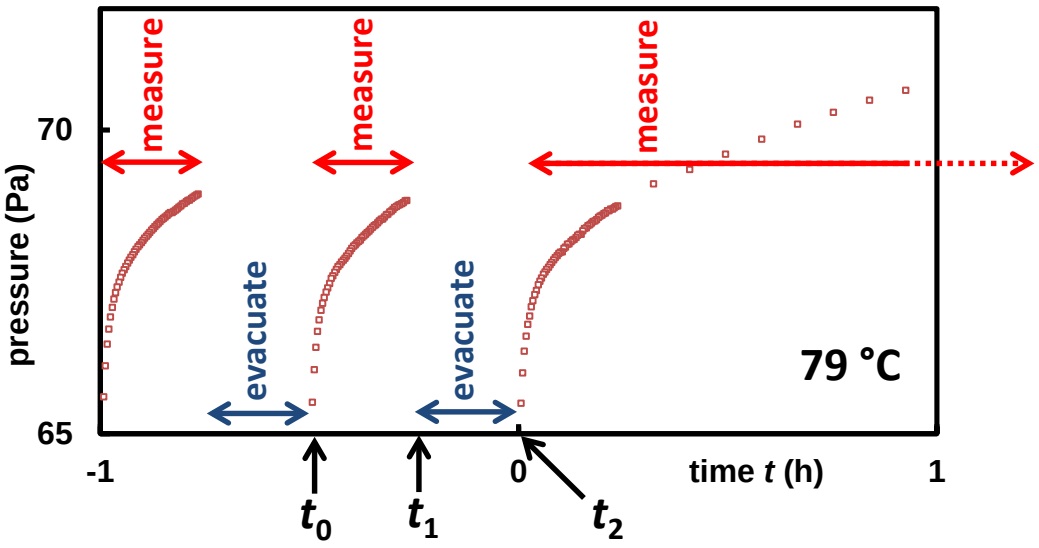

Figure 19. Cyclic pumping, followed by a long measurement of *P*(t). In periodic steady state, $P(t_0) = P(t_2)$ for each cycle.

Table 5 lists the present results for TEMAH, and Figure 20 compares them to previous results using the following reference function.

$$\frac{P_V(T)}{\text{Pa}} = 16.768 - \frac{842.7}{(T/\text{K})} + \frac{1.2655\times10^6}{(T/\text{K})^2} \qquad (25)$$

Table 5. Vapor pressures and standard uncertainties of TEMAH.

T / K	P_V / Pa		$u(P_V)$ / Pa
312.194	2.96	±	0.07
322.200	7.15	±	0.05
332.202	15.87	±	0.05
342.179	32.87	±	0.13
352.192	64.4	±	0.3
362.195	121.0	±	0.8
372.213	216	±	2
382.212	370	±	5
392.238	591	±	14

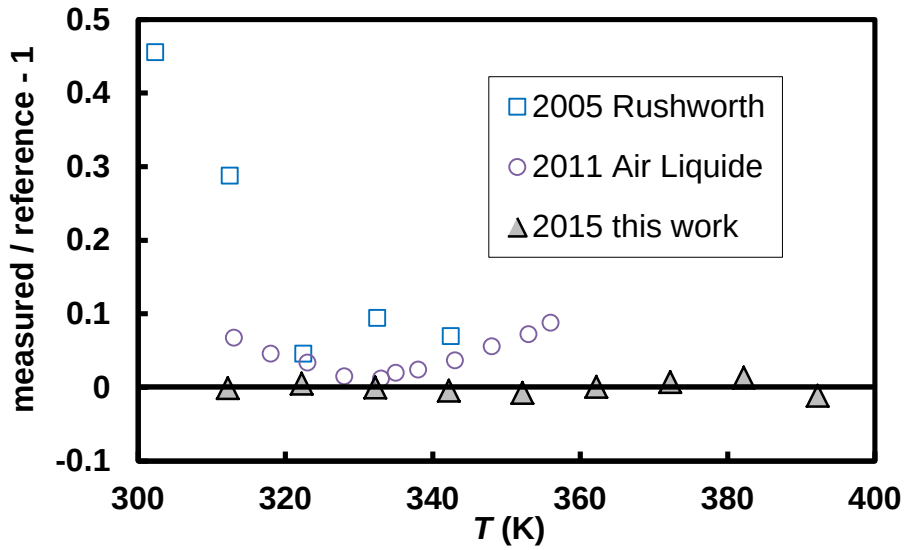

Figure 20. TEMAH results compared to data published by Rushworth et al. [38] and by Air Liquide [39]. The reference function is Eq. (25).

The relative standard uncertainty of P_V was estimated as follows.

$$\frac{u(P_V)}{P_V} = \left[\left(\frac{T}{P_V}\frac{dP_V}{dT} \right)^2 \left(\frac{u(T)}{T} \right)^2 + \left(\frac{u(P)}{P} \right)^2 + \left(\frac{u(P_{\text{fit}}(0))}{P_{\text{fit}}(0)} \right)^2 + \left(\frac{dP_{VA}}{dV_{12}} \right)^2 \left(\frac{u(V_{12})}{V_{12}} \right)^2 \right]^{1/2} \quad (26)$$

Here, the uncertainty $u(P_{\text{fit}}(0))$ is the statistical uncertainty of $P_{\text{fit}}(0)$ associated with fitting Eq. (18), and the uncertainty associated with separating P_{VA} from $P_{\text{fit}}(0)$ was obtained by multiplying the uncertainty of V_{12} by the derivative of Eq. (24) with respect to V_{12} . Table 6 shows that these two uncertainties were dominant.

Table 6. 100 times the dimensionless standard relative uncertainties: $100u(P_V)/P_V$. The four middle columns correspond to the four terms of Eq. (26).

T (K)	T	P	$P_{\text{fit}}(0)$	V_{12}	total
312.194	0.06	0.39	2.30	0.30	**2.35**
322.200	0.06	0.19	0.61	0.21	**0.67**
332.202	0.05	0.11	0.20	0.18	**0.30**
342.179	0.05	0.08	0.33	0.19	**0.39**
352.192	0.04	0.07	0.35	0.25	**0.44**
362.195	0.04	0.06	0.60	0.30	**0.67**
372.213	0.04	0.05	0.88	0.39	**0.97**
382.212	0.03	0.05	1.17	0.55	**1.30**
392.238	0.03	0.05	2.15	0.94	**2.34**

Figure 21 shows the fitted values of $P_{fit}(0)$, P_1, and the rate constants k_A, k_B, and k_D. Also shown is P_{VB}, the vapor pressure of the assumed impurity, methylethylamine, which was described approximately by [40]

$$P_{VB}(T) = (1000\ \text{Pa})10\text{^}\left[5.977 - (962.3\ \text{K})/(T - 63.3\ \text{K})\right]. \quad (27)$$

Methylethylamine was chosen because it can appear as a dominant species during atomic layer deposition with TEMAH [41]. However, the vapor was not analyzed here, so perhaps the decomposition created a different volatile impurity. For example, the unstable species *$NCH_3C_2H_5$ could have formed and decomposed to gases such as nitrogen, methane, and ethane [42]. In any case, the derivation of Eq. (18) did not depend on the number of decomposition species [17], and the fitted value of $P_{fit}(0)$ was insensitive to the assumed impurity vapor pressure P_{VB}. Increasing the value of P_{VB} by a factor of 10^4 did not change $P_{fit}(0)$ or its uncertainty. Knowing the decomposition products was not necessary to obtain the vapor pressure of TEMAH.

The curve drawn through the k_A data is an approximate Arrhenius description of the decomposition rate above 50 °C:

$$k_A(T) = (4.4\times10^4\ \text{s}^{-1})\exp\left[-(10655\ \text{K})/T\right]. \quad (28)$$

The curve drawn through the k_D data is the estimate $k_D = \pi^2 D / L^2$, where the Wilke-Chang method [24,25] was used to estimate the mass diffusivity D of methylethylamine in TEMAH, and fitting the sample depth to the data yielded the reasonable value L = 1.4 mm.

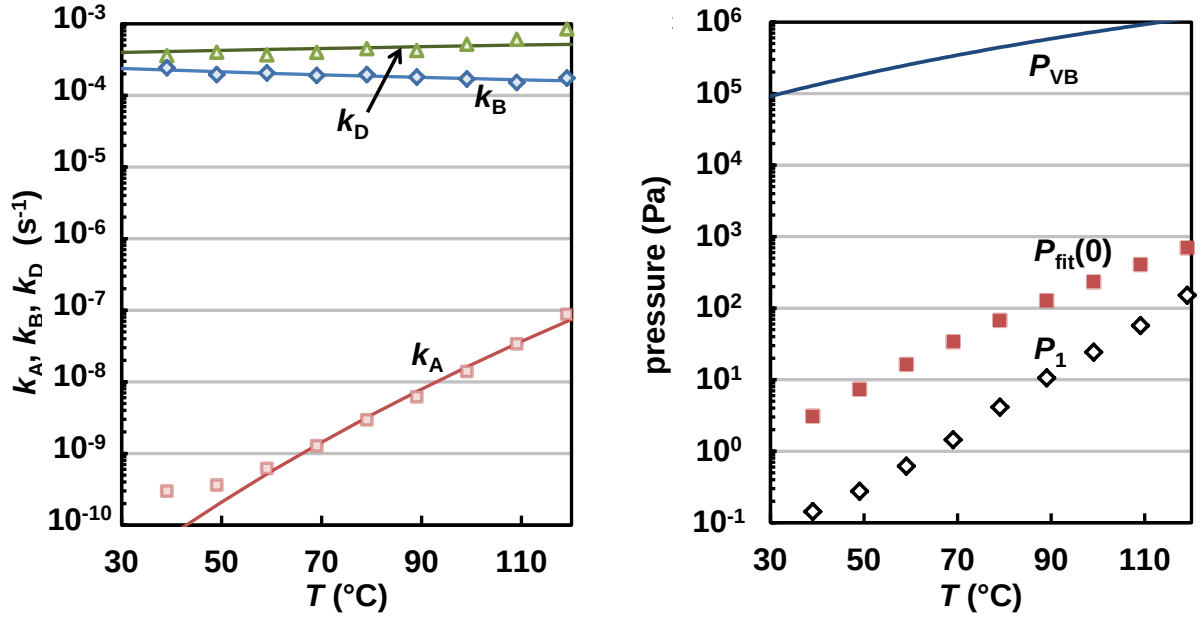

Figure 21. LEFT: Fitted values of the rate constants k_A, k_B, and k_D. The curve drawn through the k_A data is an approximate Arrhenius description of the decomposition rate, Eq. (28), and the curve drawn through the k_D data is an estimate based on the diffusivity of methylethylamine in TEMAH. RIGHT: The vapor pressure P_{VB} assumed for the impurity, Eq. (27), and the fitted values of $P_{fit}(0)$ and P_1.

7. Appendix: Degassing methods used elsewhere

Methods used to degas liquids have evolved slowly over the last 150 years; see the brief reviews that are included in articles by Markham and Kobe [43], Battino and Clever [44], and Battino and Evans [45]. See also Hickman's review of vacuum distillation [46]. As early as 1855, Bunsen used boiling followed by cooling in a vacuum. In 1928, Hibben [47] described a method of vacuum sublimation and the conditions necessary for purification; much later Bell et al. [48] published a similar method. Between 1966 and 1971, Battino and coworkers [44,45,49,50] developed a series of degassing methods, the last of which stirred a liquid while pumping the vapor space through a condenser. Battino and Clever [44] mentioned two simple methods that are still frequently used to degas liquids in the laboratory: freeze-pump-thaw and batch distillation. Here the discussion is limited to why these were inadequate for the present purpose.

In the freeze-pump-thaw method, the sample is cyclically frozen, pumped under vacuum, and then allowed to thaw while it is valved off from the vacuum pump. This method is useful for removing a gas such as air from a liquid whose vapor pressure is so large that the sample would be lost when pumped at room temperature. However, it is not effective for removing an impurity that is much less volatile than air, especially if the impurity itself is frozen. Also, if the impurity has a vapor pressure below 100 Pa, a sample with a depth of only 10 mm will have a hydrostatic pressure that will suppress the formation of impurity vapor bubbles.

In batch distillation, one boils away under vacuum all but a fraction f of the liquid. The Rayleigh distillation equation [51,52] predicts that, if a boiling liquid is in equilibrium with its vapor, the concentration x_B of the impurity will decrease by the factor

$$\frac{x_B(f)}{x_B(1)} = f^{\alpha-1}, \tag{29}$$

where α is the relative volatility defined by Eq. (10). In principle, this method would seem to be effective. For nitrogen dissolved in naphthalene at 80 °C, Eq. (29) predicts that boiling away only 0.01 % of the naphthalene (f = 0.9999) will decrease the nitrogen concentration to only 2×10^{-16} of its initial value. In practice, such improvement rarely occurs because maintaining the equilibrium state assumed by Eq. (29) is made difficult by the impurity's diffusion through the liquid. The sample cannot be stirred fast enough to ensure that the impurity concentration at the liquid-vapor interface is the same as the concentration elsewhere in the sample.

Rotating the container (Kugelrohr) is effective for a liquid sample because it creates a thin film that decreases the length for mass diffusion. Unfortunately, incorporating rotation into a bakeable all-metal apparatus designed for low pressures is difficult. The simple means of stirring the sample described in Section 4.1 had little effect.

Pumping through a semipermeable membrane for two weeks was used by Růžička et al. [24] to degas a sample of solid naphthalene. This innovative approach, which used a PDMS (polydimethylsiloxane) membrane, was effective for gases of low molecular weight. It seems unlikely that it could be used to remove a heavier hydrocarbon impurity.

8. Acknowledgements

I thank Michal Fulem and Kveta Růžička for encouragement and advice about measuring vapor pressures, Doug Meier for advice about metal organic chemistry, Kurt Benkstein for the loan of the glove box, and Jim Maslar and Don Burgess for helpful conversations. This work was funded in part by the NIST Office of Microelectronic Programs.

9. References

1. Soulet, A.; Duquesne, L.; Jursich, G.; Inman, R.; Misra, A.; Blasco, N.; Lachaud, C.; Marot, Y.; Prunier, R.; Vautier, M.; Anderson, S.; Clancy, P.; Havlicek, P. Optimizing the selection and supply of Hf precursor candidates for gate oxide. *Semiconductor Fabtech*, 27th edition **2005**, 74-81.
2. Ambrose, D. Vapor pressures. Chapter 13 in *Experimental Thermodynamics, Vol II, Experimental Thermodynamics of Non-Reacting Fluids*, Le Neindre, B.; Vodar, B. eds., Butterworths, London, 1975.
3. Ambrose, D. Vapour pressures. Chapter 7 in *Chemical Thermodynamics, Vol I*, M.L. McGlashan, senior reporter, The Chemical Society, London, 1973.
4. Verevkin, S.P.; Phase changes in pure component systems: Liquids and gases. Chapter 2 in *Measurement of the Thermodynamic Properties of Multiple Phases*, R.D. Weir and T.W. de Loos, eds., Elsevier, Amsterdam 2005.
5. Růžička, K.; Fulem, M.; Růžička, V. Vapor Pressure of organic compounds. Measurement and correlation", *http://www.vscht.cz/fch/Kvetoslav.Ruzicka/ICTP_VaporPressureGroup.pdf* (accessed Oct. 2015).
6. *Measurement of the Thermodynamic Properties of Multiple Phases*, edited by R.D. Weir, T.W. de Loos, Elsevier, 2005.
7. Raal J.D.; Mühlbauer, A.L. *Phase Equilibria Measurement and Computation*, Taylor & Francis, Washington, 1998.
8. Sasse, K.; Jose, J.; Merlin, J.; A static apparatus for measurement of low vapor pressures. Experimental results on high molecular-weight hydrocarbons. *Fluid Phase Equilib.* **1988**, 42, 287-304.
9. Tobaly, P.; An apparatus for vapor pressure measurements of organic solids using a computer controlled null-detector. *Rev. Sci. Instrum.* **1991**, 62, 2011-2015.
10. Allen, J.E.; Nelson, R.N.; Harris, B.C. Apparatus for measuring thermodynamic properties at low temperatures. *Rev. Sci. Instrum.* **1999**, 70, 4283-4294.
11. Nasirzadeh, K.; Zimin, D.; Neueder, R.; Kunz, W.; Vapor-pressure measurements of liquid solutions at different temperatures: Apparatus for use over an extended temperature range and some new data. *J. Chem. Eng. Data* **2004**, 49, 607-612.
12. Gorobei, V.N.; Krutovskikh, M.P.; Vitkovskii, O.S. Measurement methods and instruments for the saturated vapor pressure of oil products. *Meas. Tech.* **2006**, 49, 265-269.
13. Monte, M.J.S.; Santos, L.M.N.B.F.; Fulem, M.; Fonseca, J.M.S.; Sousa, C.A.D. New static apparatus and vapor pressure of reference materials: Naphthalene, benzoic acid, benzophenone, and ferrocene. *J. Chem. Eng. Data* **2006**, 51,757-766.

14. Fulem, M.; Růžička, K.; Růžička, V.; Šimeček, T.; Hulicius, E.; Pangrác, J. Vapour pressure measurement of metal organic precursors used for MOVPE. *J. Chem. Thermodyn.* **2006**, 38, 312-322.
15. Pangrác, J.; Fulem, M.; Hulicius, E.; Melichar, K.; Šimeček, T.; Růžička, K.; Moravek, P.; Růžička, V.; Rushworth, S.A. Vapor pressure of germanium precursors. *J. Cryst. Growth* **2008**, 310, 4720-4723.
16. Berg, R.F. Thermoelectric temperature control device for vapor pressure measurements. *Rev. Sci. Instrum.* **2011**, 82, 085110-6.
17. Berg, R.F. Correcting "static" measurements of vapor pressure for time dependence due to diffusion and decomposition. ~~submitted to~~ *J. Chem. Eng. Data.* **2015**, v?, p-p?.
18. Certain commercial materials or equipment are identified in this paper in order to specify the experimental procedure adequately. Such identification is not intended to imply recommendation or endorsement by the National Institute of Standards and Technology, nor is it intended to imply that the materials or equipment identified are the best available for the purpose.
19. Redhead, P.A.; Ultrahigh and extreme high vacuum. Chapter 11 in *Foundations of Vacuum Science and Technology*, edited by J. M. Lafferty, Wiley, New York, 1998.
20. Outlaw, R.A.; Tompkins J.G. *Ultrahigh Vacuum Design and Practice*, AVS, New York 2009.
21. Berg, R.F. Hydrogen traps in the outgassing model of a stainless steel vacuum chamber. *J. Vac. Sci. Technol. A* **2014**, 32, 031604-13.
22. Šetina, J.; New approach to corrections for thermal transpiration effects in capacitance diaphragm gauges. *Metrologia* **1999**, 36, 623-626.
23. Sherwood, J.N.; White, D.J. Self-diffusion in polycrystalline naphthalene. *Phil. Mag.* **1967**, 16, 975-980.
24. Wilke, C.R.; Chang, P. Correlation of diffusion coefficients in dilute solutions. *AICHe J.* **1955**, 1, 264-270.
25. Reid, R.C.; Prausnitz, J.M.; Poling, B.E. *The Properties of Gases and Liquids*, 4th edition, McGraw Hill, New York, 1987.
26. Růžička, M. Fulem, V. Růžička, "Recommended vapor pressure of solid naphthalene", *J. Chem. Eng. Data* **50**, 1956-1970 (2005).
27. D.L. Camin, F.D. Rossini, "Physical properties of fourteen API Research hydrocarbons, C9 to C15", *J. Phys. Chem.* **59**, 1173-1179 (1955).
28. L. Fowler, W.N. Trump, C.E. Vogler, "Vapor pressure of naphthalene. New measurements between 40 and 180 C 13", *J. Chem. Eng. Data* **13**, 209-210 (1968).
29. R.D. Chirico, S.D. Knipmeyer, A. Nguyen, W.V. Steele, "The thermodynamic properties to the temperature 700 K of naphthalene and of 2,7-dimethylnaphthalene", *J. Chem. Thermodyn.* **25**, 1461-1494 (1993).
30. Růžička, M. Fulem, V. Růžička, "Recommended vapor pressure of solid naphthalene", *J. Chem. Eng. Data* **50**, 1956-1970 (2005).
31. NIST Standard Reference Subscription Database 3, version 2-2012-1-Pro, *wtt-pro.nist.gov*.
32. Kaplan, L.; Kester, W.L.; Katz, J.J. Some properties of iron biscyclopentadienyl. *J. Am. Chem. Soc.* **1952**, 74, 5531-5532.

33. Edwards, J.W.; Kington, G.L. Thermodynamic properties of ferrocene. Part 2. Vapour pressure and latent heat of sublimation at 25°C by the effusion and thermistor manometer. *Trans. Faraday Soc.* **1962**, 58, 1323-1333.
34. Emel'yanenko, V.N.; Verevkin, S.P.; Krol, O.V.; Varushchenko, R.M.; Chelovskaya, N.V. Vapour pressures and enthalpies of vaporization of a series of the ferrocene derivatives. *J. Chem. Thermodyn.* **2007**, 39, 594-601.
35. Siddiqi, M.A.; Atakan, B. Combined experiments to measure low sublimation pressures and diffusion coefficients of organometallic compounds. *Thermochim. Acta* **2007**, 452, 128-134.
36. Fulem, M.; Růžička, K.; Červinka, C.; Rocha, M.A.A.; Santos, L.M.N.B.F.; Berg, R.F. Recommended vapor pressure and thermophysical data for ferrocene. *J. Chem. Thermodyn.* **2013**, 57, 530-540.
37. Rohác, V.; Růžička, K.; Růžička, V.; Zaitsau, D.; Kabo, G.; Diky, V.; Aim, K. Vapour pressure of diethyl phthalate. *J. Chem. Thermodyn.* **2004**, 36, 929-937.
38. Rushworth, S.A.; Smith, L.M.; Kingsley, A.J.; Odedra, R.; Nickson, R.; Hughes, P. Vapour pressure measurement of low volatility precursors. *Microelectron. and Reliab.* **2005**, 45, 1000-1002.
39. Air Liquide, TEMAHf data sheet, *http://www.engineering-solutions.airliquide.com/file/otherelement/pj/2d/8f/94/07/temahf1863163035765428806.pdf* (accessed Oct. 2015).
40. Wolff H.; Schiller, O. The vapour pressure behavior and the association of N-methylethylamine, diethylamine and their N-deuterioanalogues in mixtures with n-hexane. *Fluid Phase Equil.* **1985**, 22, 185-207.
41. Sperling, B.A.; Kimes, W.A.; Maslar, J.E.; Chu, P.M. Time-resolved Fourier transform infrared spectroscopy of the gas phase during atomic layer deposition. *J. Vac. Sci. Techol. A* **2010**, 28, 613-621.
42. Růžička, K. private communication **2015**.
43. Markham, A.E.; Kobe, K.A. The solubility of gases in liquids. *Chem. Rev.* **1941**, 28, 519-588.
44. Battino, R.; Clever, H.L. The solubility of gases in liquids. *Chem. Rev.* **1966**, 66, 395-463.
45. Battino, R.; Evans, F.D. Apparatus for rapid degassing of liquids. *Anal. Chem.* **1966**, 38, 1627-1629.
46. Hickman, K.C.D.; High-vacuum short-path distillation - A review. *Chem. Rev.* **1944**, 28, 51-106.
47. Hibben, J.H. Removal of dissolved gases from liquids by vacuum sublimation. *Bur. Stand. J. Res.* **1928**, 3, 97-104.
48. Bell, T.N.; Cussler, E.L.; Harris, K.R.; Pepela, C.N.; Dunlop, P.J. An apparatus for degassing liquids by vacuum sublimation. *J. Phys. Chem.* **1968**, 72, 4693-4695.
49. Battino, R.; Evans, F.D.; Bogan, M. Apparatus for the rapid degassing of liquids. Part II. *Anal. Chem. Acta* **1968**, 43, 520-522.
50. Battino, R.; Banzhof, M.; Bogan, M.; Wilhelm, E. Apparatus for rapid degassing of liquids. Part III. *Anal. Chem.* **1971**, 43, 806-807.

51. Halvorsen, I.J.; Skogestad, S. Theory of distillation. *Encyclopedia of Separation Science, Volume II*, edited by I.D. Wilson, E.R. Adlard, M. Cooke, C.F. Poole, Academic Press, 2000.
52. Seader, J.D.; Siirola, J.J.; Barnicki, S.D.; Distillation, chapter 13 in *Perry's Chemical Engineers' Handbook*, edited by R.H. Perry, D.W. Green, J.O. Maloney, McGraw-Hill, New York, 1997.

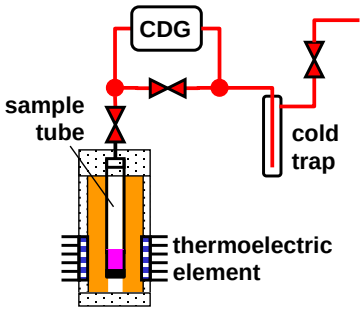

Figure 22. For Table of Contents use only. (R.F. Berg, Apparatus to measure the vapor pressure of slowly decomposing compounds from 1 Pa to 10^5 Pa)